Distortion Mechanisms in Varactor Diode-Tuned Microwave Filters

Bruce E. Carey-Smith and Paul A. Warr

***Abstract*—This paper examines the broadband distortion behavior in flexible filters employing varactor-diode tuning elements. Series- and parallel-resonant varactor-loaded transmission-lines, both commonly used in bandpass and bandstop microwave filters, are analyzed. Nonlinear Volterra-series analysis is employed to determine the second- and third-order distortion ratios dependent on the frequencies of the incident signals. It is shown that in a bandpass filter (employing parallel tuned resonators), maximum distortion occurs in the passband, while in a bandstop filter (employing series tuned resonators), minimum distortion occurs at the minimum-loss passband. The analysis is verified by practical measurement of filters employing the two modes of resonators.**

***Index Terms*—Distortion, microwave filters, tunable filters.**

I. Introduction

THE USE of semiconductor devices as tuning elements in flexible filters is attractive, as they are economical and easily integrated into miniature circuits. However, because their inherent transfer characteristics are nonlinear, they distort the incident signals.

Tunable filters must be judged according to their linearity since their primary purpose is to either remove the signals that could cause distortion or to remove the distortion itself.

In order to arrive at useful conclusions about the characteristics of the distortion within semiconductor-tuned filters, it is necessary to have an understanding of the nonlinear behavior of the circuit elements and subsystems. Firstly, an examination of the nonlinear properties of two of the most common semiconductor devices used as the tuning components in microwave filters is presented. This leads to a detailed analysis of two varactor-tuned transmission-line resonator topologies, which are the common subsystems within tunable bandpass and bandstop filters (BSFs). The linear and nonlinear properties of these resonators are examined in order to draw conclusions about the nonlinear performance of their associated filters.

In filters that contain semiconductor elements, the nonlinearity is not memoryless and, thus, the method of describing it must incorporate time-dependent circuit information, making Taylor-series analysis inadequate.

The Volterra series is employed for the nonlinear analysis in this paper, as it is suitable for modeling memory effects. Its elements (or "kernels") are progressively higher order convolution integrals encompassing greater numbers of excitation signals [1].

Manuscript received October 31, 2005; revised March 3, 2006.

The authors are with the Centre for Communications Research, University of Bristol, Bristol BS8 1UB, U.K. (e-mail: ccr-wireless@bristol.ac.uk).

Digital Object Identifier 10.1109/TMTT.2006.881024

Narrowband distortion measurements of tunable resonators [2] and filters [3] have been reported previously. In contrast, this paper focuses on broadband performance, using mathematical analysis to explain the observed trends in nonlinearity.

II. Semiconductor Elements in Tunable Microwave Filters

In order to establish the distortion produced in semiconductor-tuned filters, the mechanisms by which it is generated in the components should be examined. The most common semiconductor devices used as tuning elements in microwave filters are varactor and p-i-n diodes. It is established here that the contribution of varactor diodes to the nonlinear characteristics is highly dominant over p-i-n diodes.

A. p-i-n Diodes

p-i-n diodes are constructed by sandwiching a relatively thick layer of intrinsic semiconductor material between a pn junction. The device behaves like a current controlled resistance to high-frequency signals. Provided there is sufficient dc-bias current, p-i-n diodes will display almost linear behavior for small RF signals. As long as the displacement of junction charge due to the high-frequency excitation is much smaller than the stored charge due to the dc bias, the high-frequency resistance of the junction will not be modulated by the high-frequency signal [4].

It is shown in [5] that the stored charge Q_s and the charge due to the incident RF signal q_s in the intrinsic layer is given as follows by (1) and (2), respectively:

$$Q_s = I_F \tau \tag{1}$$

$$q_s = \frac{i_f}{\pi f_c} \tag{2}$$

where I_F is the forward bias current, τ is the minority charge carrier lifetime, and the RF signal has frequency f_c and amplitude i_f.

Since it is desirable that Q_s be much greater than q_s, an expression for the relative magnitude of required forward bias current can be found as

$$\frac{I_F}{i_f} >> \frac{1}{\tau \pi f_c}. \tag{3}$$

Typical small-signal RF p-i-n diodes have charge carrier lifetimes in the order of 300 ns–1.5 μs. The logarithmic ratio representing the level of RF modulation of the stored charge is plotted in Fig. 1 for an RF carrier frequency of 800 MHz. The equivalent series resistance R_s is dominated by a proportional relationship to $1/Q_s$ so that any variation in the overall stored charge in the

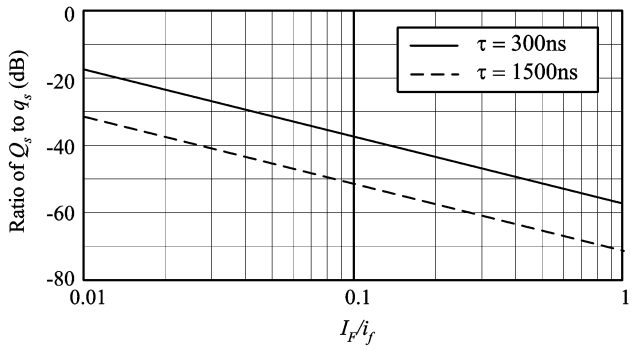

Fig. 1. Relative level of high-frequency charge displacement q_s against normalized bias current I_F/i_f.

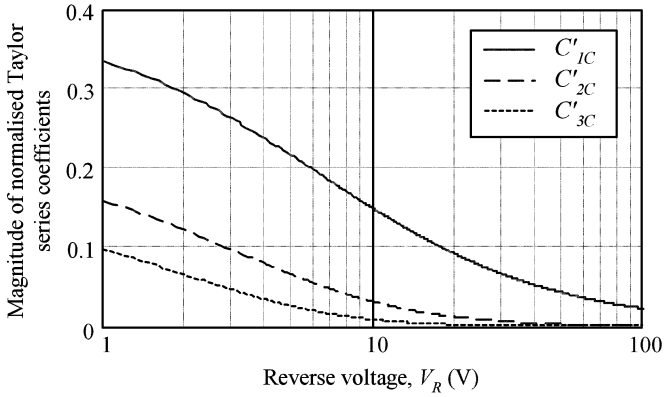

Fig. 2. Normalized coefficients for a Taylor-series expansion of depletion capacitance around dc-bias point V_R.

p-i-n diode junction will result in modulation of the resistance. This is a nonlinear effect and will cause distortion. However, from Fig. 1, it can be seen that, when the RF signal is small, it is relatively easy to provide enough forward bias current to reduce the variation in Q_s below 40 dB.

If designed correctly, p-i-n diodes will not introduce levels of distortion that are significant in all but the most sensitive applications. For this reason, they will not be considered further in this paper. However, I_F should be maintained at a sufficient level; this may be an issue in certain low-power applications.

B. Varactor Diodes

A varactor diode is a voltage-controlled device. The reverse-biased junction capacitance can be adjusted by varying the reverse-biased voltage. Two main components make up the capacitance across the semiconductor junction: diffusion and depletion capacitance. Diffusion capacitance is dominant under forward bias and is due to the injected minority charge in the junction. Under reverse bias, this injected charge tends to zero and the depletion capacitance becomes dominant. The depletion capacitance is due to the stored charge in the depletion region and is influenced by the magnitude of the reverse-bias voltage. The equation that describes the depletion capacitance is [6]

$$C_j = \frac{C_{j0}}{\left(1+\frac{v_R}{V_j}\right)^{m_j}} \tag{4}$$

where C_{j0} is the zero-bias junction capacitance, v_R is the reverse-bias voltage, and V_j is the junction potential, which is related to the thermal voltage and doping levels of the junction. m_j is the junction grading or doping coefficient and varies between 0.33 (linear junction) and 5.0 (hyper-abrupt junction) depending on the doping profile.

The varactor diode depletion capacitance can be directly modulated by an RF signal. Since the depletion capacitance is a nonlinear function of reverse-bias voltage, this modulation will result in distortion products being generated.

The depletion capacitance nonlinearity can be modeled by a memoryless Taylor-series expansion around the dc-bias point. Weak nonlinearities, as seen in small-signal varactor diodes, typically have small variation around a quiescent point and can be described with good accuracy by only a few terms in the Taylor series.

The Taylor series expansion of the depletion capacitance $C_{j\mathrm{NL}}$ is given by

$$C_{j\mathrm{NL}}(v_R) = C_j + C_{j1}v_r + C_{j2}v_r^2 + C_{j3}v_r^3 + \cdots + C_{jn}v_r^n \tag{5}$$

where C_j is given by (5) and the coefficients C_{j1}–C_{jn} are given by the nth-order derivative of C_j

$$C_{jn} = \frac{1}{n\,!}\left.\frac{d^n C_j(v_R)}{dv_R^n}\right|_{v_R=V_R}. \tag{6}$$

The terms V_R and v_r are the dc and ac components of the reverse-bias voltage v_R.

The coefficients can be normalized to the dc or linear component so that

$$C'_{jn} = \frac{1}{n!C_j(V_R)}\left.\frac{d^n C_j(v_R)}{dv_R^n}\right|_{v_R=V_R}. \tag{7}$$

The magnitude of the first- and second-order normalized coefficients is plotted in Fig. 2 for a typical small-signal varactor diode with $m_j = 2.42, V_j = 6.22$ V and $C_{j0} = 9.12$ pF. The depletion capacitance of the varactor diode decreases with increasing reverse bias. Fig. 2 indicates that for larger values of reverse voltage (and, hence, lower varactor capacitance), the relative level of distortion reduces.

The remaining analysis and discussion in this paper is concerned with varactor diodes and their impact on linearity within the context of tunable filters. Despite recent advances in topologies to lower the distortion generated in varactor diodes [7], this element will continue to dominate the observed distortion.

III. Distortion Analysis of Varactor Tuned Filters

The common building blocks used in semiconductor tunable microwave filters are the varactor diode and the transmission line. Used together they can be connected to form a relatively high-Q resonant circuit whose resonant frequency can be tuned by altering the varactor bias voltage. Both series and parallel resonant structures can be formed in this way. Two of the most commonly used structures are shown in Fig. 3.

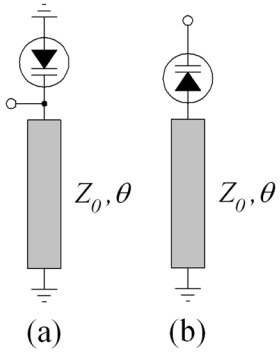

Fig. 3. Varactor-tuned transmission-line resonators. (a) Parallel resonant. (b) Series resonant.

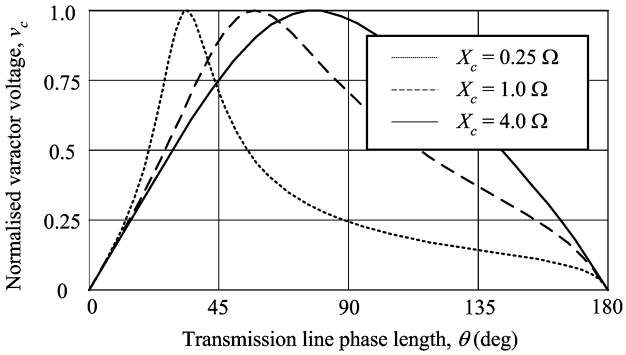

Fig. 4. Magnitude of the voltage across the varactor diode in a parallel-resonant varactor-loaded transmission line. The specified value of X_c corresponds to the transmission-line quarter-wavelength.

In order to study distortion in filter structures, it is of benefit to analyze these simple resonant structures when driven from a resistive source. Of particular interest is the voltage developed across the varactor diode since this contributes directly to the distortion.

A. AC Analysis of Parallel Resonant Varactor- Tuned Structure

By undertaking simple ac analysis of the parallel resonant configuration in Fig. 3(a), it is possible to plot the voltage across the varactor diode. Fig. 4 shows the magnitude of the ac voltage across the varactor v_c versus the phase length of the transmission line for several values of capacitive reactance X_c. Source voltage and resistance and transmission-line impedance are set to unity.

The point of maximum voltage corresponds to the parallel resonant condition when the impedance of the resonator approaches infinity. Since the distortion induced in the varactor due to modulation of the depletion capacitance is proportional to the ac voltage across it, for a fixed value of dc bias, the point of maximum distortion will always correspond to the parallel resonant frequency of the resonator. Resonators whose primary resonant mode is high impedance are used widely in bandpass filter design. This is the most common form of varactor-tuned filter [8]–[10]. In this case, using filter transfer function terminology, the maximum distortion will occur at the transmission pole frequencies, which are distributed across, and define, the passband of the filter. Conversely, minimum distortion will occur at the attenuation poles of the filter, which are independent of the value

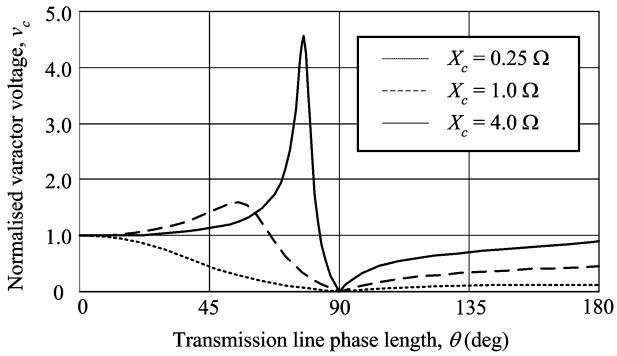

Fig. 5. Magnitude of the voltage across the varactor diode in a series-resonant varactor-loaded transmission line. The specified value of X_c corresponds to the transmission-line quarter-wavelength.

of capacitive loading. These attenuation poles correspond to the half-wavelength frequency of the transmission lines.

The maximum voltage across the varactor remains constant in the parallel configuration, regardless of capacitance value. This means that the distortion in the filter passband will follow the relationship shown in Fig. 2, decreasing for larger capacitive reactance.

B. AC Analysis of Series Resonant Varactor-Tuned Structure

A simple ac analysis can also be performed on the series resonator configuration shown in Fig. 3(b). The voltage information for this topology is shown in Fig. 5.

The series resonant mode occurs when there is maximum voltage across the varactor. At this point, the resonator impedance approaches zero and the distortion introduced by the varactor diode will be highest. This type of resonator is used predominantly in BSFs [11], [12] leading to the important conclusion that maximum distortion will occur when the excitation signals are at the center of the stopband.

The grounded transmission-line series topology has the characteristic that its point of maximum impedance will always occur at the frequency where the transmission line is a quarter-wavelength. At this frequency, the voltage across the varactor is at a minimum, independent of the actual value of capacitive reactance. This relationship can be seen mathematically by deriving the expression for the voltage across the varactor when the resonator is loaded with a resistance $R_L = R_s$. In this situation, the voltage across the varactor is given by

$$V_C = V_s \frac{-jX_C}{R_L + j2(Z_0 \tan\theta - X_C)}. \tag{8}$$

The magnitude of this function is at a maximum at resonance, when $X_C = Z_0\ tan\theta$, and drops to zero when $\theta = \pi/2$, as the transmission-line impedance tends to infinity.

Referring to Fig. 5, as the capacitive reactance is increased, and the series resonant point moves toward the quarter-wavelength frequency of the transmission line, the maximum voltage across the varactor also increases. This would lead to an increase in distortion generated by the varactor. However, recalling the

discussion on normalized coefficients for the Taylor series expansion of the depletion capacitance in Section II-B, this increase will be partially offset by the decrease in distortion as the bias voltage is increased to bring about the change in varactor capacitance.

C. Volterra-Series Analysis of Varactor-Loaded Transmission-Line Resonators

Here we use the Volterra-series approach to describe the varactor-loaded transmission-line resonators of Fig. 3. The analysis is developed from the form given in [12].

1) Parallel Resonant Topology: The Volterra kernels, which describe the parallel resonant circuit configuration, can be derived by summing the currents in the circuit such that

$$i_s(t) = v_c(t)(G_s - jY_0 \cot\theta) + C_j \frac{d}{dt}\left(v_c(t) + C'_{j1} v_c^2(t) + C'_{j2} v_c^3(t) + \cdots\right) \quad (9)$$

where C_j is given by (4) with $v_R = V_R$, v_c is the voltage across the varactor, G_s is the voltage source conductance, and the normalized Taylor series coefficients C'_{j1}, C'_{j2} etc. are found from (7).

Due to the charge being less than unity and the decreasing size of the capacitance coefficients, the terms in (9) quickly diminish in magnitude as their order increases. In order to simplify the following analysis, the capacitance function is limited to third order, under the assumption that the higher order components will have only modest effect on the results.

The nonlinear transfer functions are found sequentially by exciting the circuit with an increasing numbers of noncommensurate frequency tones and solving (9) for the voltage $v_c(t)$ [7]. Only the contributions that relate to the particular transfer function being solved need be considered. The first-, second-, and third-order transfer functions for the parallel configuration resonant circuit are given by

$$H_1(\omega) = \frac{1}{G_s - jY_0 \cot\theta + j\omega C_j} \quad (10)$$

$$H_2(\omega_a, \omega_b) = -j(\omega_a + \omega_b) \frac{C_j C'_{j1} H_1(\omega_a) H_1(\omega_b)}{G_s - jY_0 \cot\theta + j(\omega_a + \omega_b) C_j} \quad (11)$$

and

$$H_3(\omega_a, \omega_b, \omega_c) = \frac{1}{3} \frac{2C_j C'_{j1} |\{HH_{12}\}| + 3C_j C'_{j2} |\{HH_3\}|}{G_s - jY_0 \cot\theta + j(\omega_a + \omega_b + \omega_c) C_j} \quad (12)$$

where

$$\{HH_{12}\} = (\omega_a + \omega_b + \omega_c) \cdot [H_1(\omega_a) H_2(\omega_b, \omega_c) + H_1(\omega_b) H_2(\omega_a, \omega_c) + H_1(\omega_c) H_2(\omega_a, \omega_b)] \quad (13)$$

and

$$\{HH_3\} = (\omega_a + \omega_b + \omega_c) \cdot [H_1(\omega_a)\ H_1(\omega_b)\ H_1(\omega_c)]. \quad (14)$$

Using these functions, it is possible to calculate any first-, second-, or third-order signal component by selecting the appropriate values for ω_a, ω_b and ω_c.

The parallel resonant configuration finds greatest application in bandpass filters. In this context, the primary concern, when dealing with nonlinearity, will be situations where distortion products fall within the passband of the filter. In this case, the distortion products have the potential to reduce the integrity of the wanted signal. Where distortion products fall in the stopband, they will generally be attenuated sufficiently to avoid any detrimental impact on performance.

a) Third-Order Intermodulation Distortion (IMD): Both even- and odd-order distortion can potentially generate products in-band, depending on the spectral location of the exciting signals. The component of greatest interest is the third-order IMD, which produces distortion products near to the excitation signals. The relative magnitude of the third-order intermodulation components can be found from the ratio of (10) and (11) by setting ω_a and ω_b equal to ω_1, and ω_c equal to $-\omega_2$, or vice versa.

The third-order intermodulation rejection ratio (3IMRR) for the third-order component at $2\omega_1 - \omega_2$ is given by

$$3\text{IMRR} = \frac{3}{8} A_s^2 \frac{|H_3(\omega_1, \omega_1, -\omega_2)|}{|H_1(\omega_1)|} \quad (15)$$

where A_s is the magnitude of the tones used to excite the circuit. The two tones are assumed to have equal amplitude. The third-order component at $2\omega_1 - \omega_2$ can be found by interchanging ω_1 and ω_2 in (15).

Equation (15) is used to determine the relative level of the third-order intermodulation component for a typical small-signal varactor diode connected in parallel with a 90-Ω transmission line and driven from a 50-Ω source. The results are shown in Fig. 6. The excitation signals were swept such that either the upper or lower third-order intermodulation product occurred at the parallel resonant frequency of the resonator. The circuit was tuned such that the parallel resonant frequency occurred at 600 MHz and the transmission-line half-wavelength occurred 2.06 GHz. The required varactor-bias voltage V_R was 0.55 V.

An equivalent parallel resonant circuit was built using an Infineon BB857 varactor diode and a grounded section of 90-Ω microstrip fabricated on low-loss microwave laminate ($h = 1.52$ mm, $\varepsilon_r = 3.05, \tan\delta = 0.003$). Using a buffered two-tone source at -1.4 dBm per tone, the third-order IMD was measured at the circuit input using a directional coupler and high dynamic-range spectrum analyzer. The results are plotted in Fig. 6.

The difference in the measured and modeled results is due to two factors. Firstly, a resonance associated with the varactor diode bias network is causing reduction in low-frequency distortion. Secondly, the parasitic inductance of the varactor diode results in the frequency of the second parallel resonance being reduced below that of the transmission-line half-wavelength. This effect lowers the measured distortion above the primary parallel resonance.

The significant point, however, is that the maximum distortion occurs as the two excitation signals converge on the parallel resonant frequency. Conversely, distortion is at a minimum

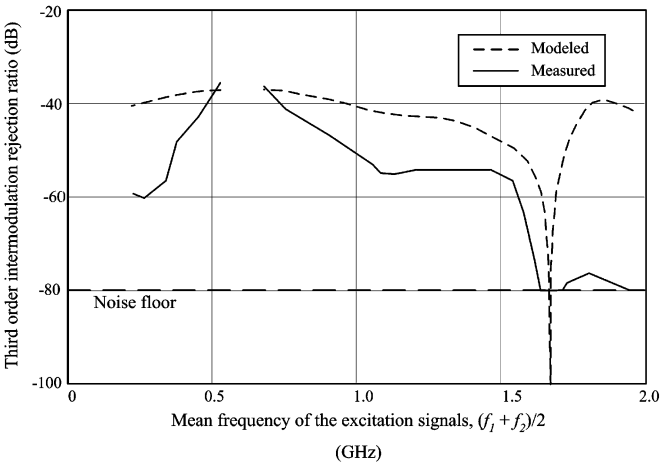

Fig. 6. Third-order IMD component relative to the excitation signal in a varactor-tuned parallel transmission-line resonator.

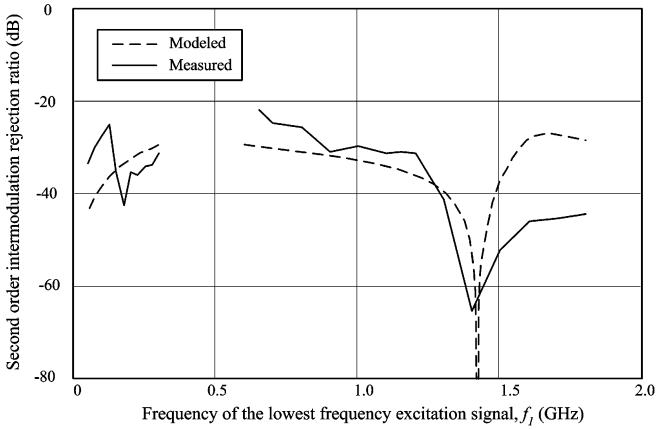

Fig. 7. Second-order IMD relative to excitation signal. The excitation signal consists of two equal amplitude tones spaced so that the intermodulation component always falls at the parallel resonant frequency.

when the excitation signals coincide with the transmission-line half-wavelength frequency. The first significant null in the magnitude of the third-order distortion products at the parallel resonant frequency occurs when the upper of the two excitation signals is coincident with the transmission-line half-wavelength frequency. The increase in magnitude above this point is due to the upper excitation signal reaching the second parallel resonance of the circuit.

b) Second-Order IMD: The two second-order intermodulation components generated from a two-tone excitation signal will occur at $(\omega_2+\omega_1)$ and $(\omega_2-\omega_1)$. The second-order intermodulation rejection ratio (2IMRR) for the second-order component at $(\omega_2+\omega_1)$, neglecting higher order components, is given by

$$2\mathrm{IMRR}=\frac{1}{2}A_s\frac{|H_2(\omega_1,\omega_2)|}{|H_1(\omega_1)|} \tag{16}$$

where A_s is the magnitude of the tones used to excite the circuit. The second-order component at $(\omega_2-\omega_1)$ can be found by reversing the sign of ω_1 in (16).

Using the same setup as described in Section III-C.1a, the relative level of the second-order IMD products was calculated and measured. Again, the excitation signals were swept such that either the upper or lower second-order IMD product ($\omega_2+\omega_1$ or $\omega_2-\omega_1$) occurred at the parallel resonant frequency of the resonator. The results are given in Fig. 7. Note that, in this case, the rejection ratio is plotted against the frequency of the lowest excitation tone.

Maximum second-order IMD occurs when either of the excitation tones approaches either the first or second parallel resonant frequency of the circuit. A null occurs when the higher excitation tone ω_2 reaches the half-wavelength of the transmission line. The data is discontinuous between 0.3–0.6 GHz because the distortion products cannot fall at the parallel resonant frequency when the lowest frequency tone is between these values. Although the level of the second-order IMD component is higher than that of the third (see Fig. 6) when a resonator of this topology is used in a filter, the second-order products are not so important. To generate in-band second-order distortion, at least one of the excitation tones must be far from the parallel resonant frequency, which, in the case of a bandpass filter, will result in considerable attenuation.

2) Series Resonant Topology: The analysis of the series resonant circuit of Fig. 3(b) is similar to the parallel resonant topology of Fig. 3(a). However, it is simplified by describing the voltage across the varactor as a function of charge. In this way, the voltages in the circuit can be summed such that

$$v_s(t)=i_c(t)(R_s+jZ_0\tan\theta)+q(t)S_1+q^2(t)S_2+q^3(t)S_3+\cdots \tag{17}$$

where S_1, S_2, and S_3 are first-, second-, and third-order nonlinear coefficients of the capacitor's elastance and $q(t)$ is given by the time integral of the current from ∞ to t.

The elastance coefficients can be found by rearranging the equation for depletion charge (4) [14]

$$Q_d=Q_{j0}\left(1+\frac{v_R}{V_j}\right)^{1-m_j} \tag{18}$$

to give reverse voltage v_R as a function of charge Q_d, and then differentiating with respect to charge. The first- and second-order nonlinear coefficients are thus given by

$$S_1=\frac{V_j}{Q_{j0}(1-m_j)}\left(1+\frac{v_R}{V_j}\right)^{m_j} \tag{19}$$

and

$$S_2=\frac{V_j m}{Q_{j0}^2(1-m_j)^2}\left(1+\frac{v_R}{V_j}\right)^{2m_j-1}. \tag{20}$$

The first-, second-, and third-order transfer functions can be found in a similar manner described in Section III-C.1. They are given by

$$H_1(\omega)=\frac{j\omega}{j\omega R_s+S_1-\omega Z_0\tan\theta} \tag{21}$$

$$H_2(\omega_a,\omega_b) = \frac{j(\omega_a+\omega_b)}{\omega_a\omega_b} \times \frac{S_2 H_1(\omega_a)H_1(\omega_b)}{j(\omega_a+\omega_b)R_s + S_1 - (\omega_a+\omega_b)Z_0\tan\theta} \quad (22)$$

and

$$H_3(\omega_a,\omega_b,\omega_b) = \frac{2S_2|\{HH_{12}\}| + 3S_3|\{HH_3\}|}{3(\omega_a+\omega_b+\omega_c)(jR_s - Z_0\tan\theta) + S_1} \quad (23)$$

where

$$\{HH_{12}\} = (\omega_a+\omega_b+\omega_c) \cdot \left[\frac{H_1(\omega_a)H_1(\omega_b,\omega_c)}{\omega_a(\omega_b+\omega_c)} + \frac{H_1(\omega_b)H_1(\omega_a,\omega_c)}{\omega_b(\omega_a+\omega_c)} + \frac{H_1(\omega_c)H_1(\omega_a,\omega_b)}{\omega_c(\omega_a+\omega_b)}\right] \quad (24)$$

and

$$\{HH_3\} = (\omega_a+\omega_b+\omega_c)\cdot\frac{H_1(\omega_a)H_1(\omega_b)H_1(\omega_c)}{\omega_a\omega_b\omega_c}. \quad (25)$$

a) Second-Order IMD: In contrast to bandpass filters, the second-order IMD generated by the varactor diode is important when considering the application of BSFs. If the IMD product of two high-level interfering signals falls in the band of interest, it is possible that it may inhibit the detection of the wanted signal. The worst case scenario occurs when at least one of the interferers is located at the center of the filter stopband, which is likely since the purpose of the BSF is to attenuate interfering signals.

The 2IMRR for the transmission-line grounded topology can be found from the ratio of the first- and second-order currents, which, with the appropriate excitation, can be written in terms of the magnitude of the excitation signals A_s and the first- and second-order transfer functions from (20) and (21)

$$2\text{IMRR} = \frac{1}{2}A_s\frac{|H_2(\omega_1,\omega_2)|}{|H_1(\omega_1)|}. \quad (26)$$

The second-order IMD results for the series configuration are plotted in Fig. 8. The graph shows the two-tone second-order IMD performance when one of the tones occurs at the series resonant frequency and the other is swept across frequency. The same circuit components and test setup as described in Section III-C.1a were used with the exception that the transmission-line quarter-wavelength frequency was set at 1.36 GHz. The varactor capacitance was tuned such that the series resonance occurred at 1.0 GHz ($V_R = 17.9$ V).

Maximum second-order distortion occurs at 2 GHz when both excitation tones occur close to the series resonant frequency. At this frequency, there will be maximum current flowing through the varactor diode and maximum voltage across it.

The second-order IMD passes through a null at the quarter-wavelength frequency. At this point, the transmission line presents high impedance, inhibiting the flow of distortion current. The null at 0.36 GHz is also related to the quarter-wavelength and occurs when the second tone reaches this quarter-wavelength frequency.

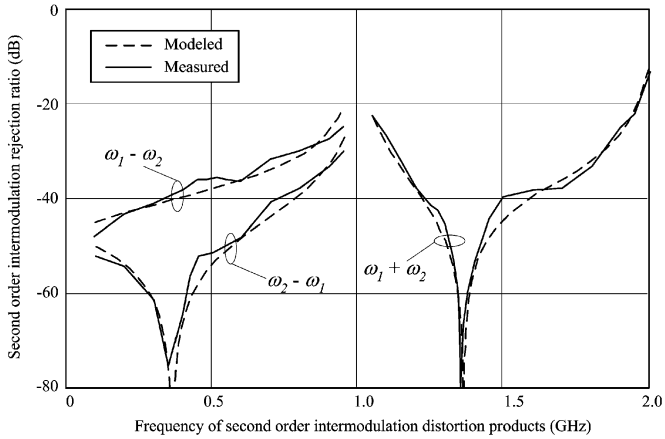

Fig. 8. 2IMRR of the series resonator topology. The excitation signal comprises two equal-amplitude tones. The first, i.e., ω_1, is held at the series resonant frequency of the resonator while the other, i.e., ω_2, is swept above and below the first.

b) Third-Order IMD: The highest level of third-order IMD occurs when at least one of the excitation signals is located at the series resonant frequency. The relative level of the third-order intermodulation components at $2\omega_1 - \omega_2$ and $2\omega_1 - \omega_2$ can be found by substituting (21) and (23) into (15). The modeled and measured results for both components are shown in Fig. 9.

The response of the $2\omega_1 - \omega_2$ component is virtually symmetrical around the series resonant frequency. It reaches a minimum at 0.64 and at 1.36 GHz; in the first case, when the excitation signal ω_2 passes through the quarter-wavelength frequency of the transmission line, and in the second case, when the distortion product itself passes through that frequency. The $2\omega_2 - \omega_1$ component reaches a minimum at 1.36 GHz when it passes through the quarter-wavelength frequency of the transmission line. A second minimum occurs at 1.72 GHz (not shown) when the excitation tone ω_2 reaches that frequency. Below the series resonant frequency, the $2\omega_2 - \omega_1$ component exhibits a gentle decay in the absence of any resonances.

The results presented in Fig. 9 have significant implications for BSFs constructed using the varactor-coupled transmission-line resonators from Fig. 3(b). In this context, maximum distortion will be generated in the resonator when the excitation tones occur in the stopband of the filter, which will be their likely location. However, in many applications, the concern over distortion is its masking effect of a wanted signal. The results above show that if the minimum loss passband (transmission-line quarter-wavelength frequency) can be designed to coincide with the wanted signal band, then the second- and third-order distortion products occurring in this frequency band will be minimized.

IV. Distortion Measurements of Varactor-Tuned Filters

To verify the wideband distortion analysis above and to extend previous reported narrowband measurements [3], a

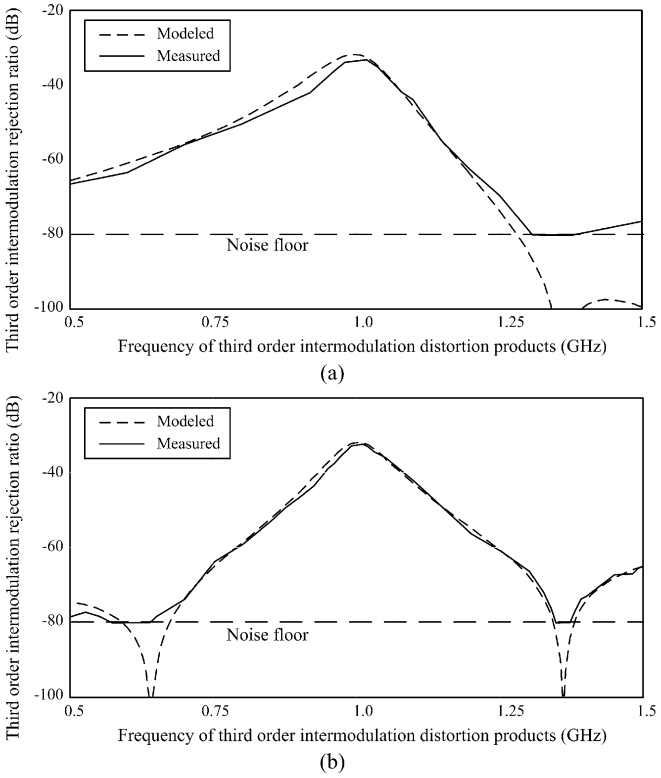

Fig. 9. Third-order IMD components: (a) $2\omega_2 - \omega_1$ and (b) $2\omega_1 - \omega_2$ relative to the fundamental component of the current in a series-resonant varactor-tuned transmission line. The excitation signal comprises two equal-amplitude tones. The first, i.e., ω_1, is held at the series resonant frequency of the resonator, while the other, i.e., ω_2, is swept above and below the first.

combline bandpass filter using parallel-coupled transmission-line resonators and a BSF comprising two series-coupled transmission-line resonators coupled via a quarter-wave through-line were constructed and measured.

A five-element varactor-tuned combline filter was constructed in microstrip to give a 5% fractional bandwidth between 1.8–2.1 GHz. The filter employed resonators with commensurate length and width, short circuited at one end and terminated in a series combination of a lumped 1.2-pF capacitor and varactor (Infineon BB839) capable of tuning between 1–18 pF. In order to gather third-order IMD data on the constructed filter, two equal-amplitude interfering signals were introduced at the filter input and the amplitude of the third-order distortion product was measured at the output. The relationship between the frequencies of the two interfering signals was chosen so that the distortion product would always fall within the passband of the filter. The results are shown in Fig. 10 for two filter tuning positions, i.e., 1.85 and 2.0 GHz.

The measured results agree with the analysis of Section III-C.1a. The increase in distortion level at the lower center-frequency tuning position follows from the results of Section III-A, where it was shown that, as the reactance of the varactor increases in proportion to the transmission-line impedance, the voltage across the varactor will increase, leading to more distortion.

In most cases, a BSF will be used to reduce the level of a large unwanted signal. This means that there will be at least one

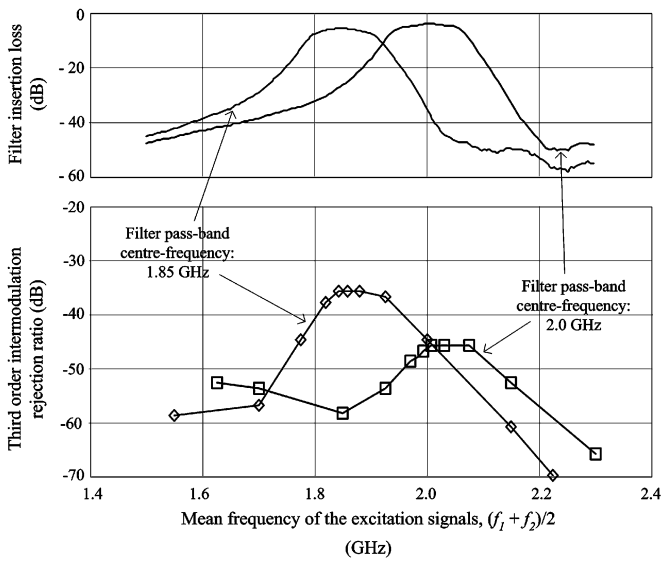

Fig. 10. Measured third-order IMD plotted against mean interference frequency for two filter tuning positions. The filter insertion loss for each tuning point is also shown.

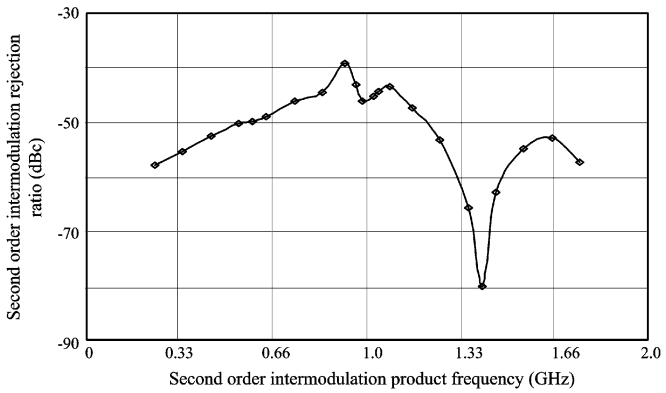

Fig. 11. Measured second-order IMD ($f_1 - f_2$ and $f_1 + f_2$) of a varactor-tuned BSF relative to the excitation signal power at the input. The excitation signal comprises two equal-amplitude tones. The first is held at the filter stopband, while the other is swept above and below the first.

large signal located in the stopband. Second-order IMD measurements were made on a varactor tuned BSF, and the results are shown in Fig. 11 for a two-tone excitation signal. Where needed in order to maintain the dynamic range of the measurement, a tunable notch filter was used to attenuate the excitation tones after the filter under test. Resistive attenuators were placed on either side of this notch filter to minimize its loading effect. The constructed filter was an inverter coupled two-element BSF formed from varactor-coupled quarterwave-length resonators of the form shown in Fig. 3(b). The construction details of this filter may be found in [12].

The results show the same general trend as those calculated theoretically using Volterra series (see Fig. 8). The minimum second-order intermodulation level occurs at the quarter-wavelength of the resonator transmission line (in this case, 1.41 GHz) and the maximum occurs around the stopband of the filter. The local minimum at the stopband center frequency occurs because

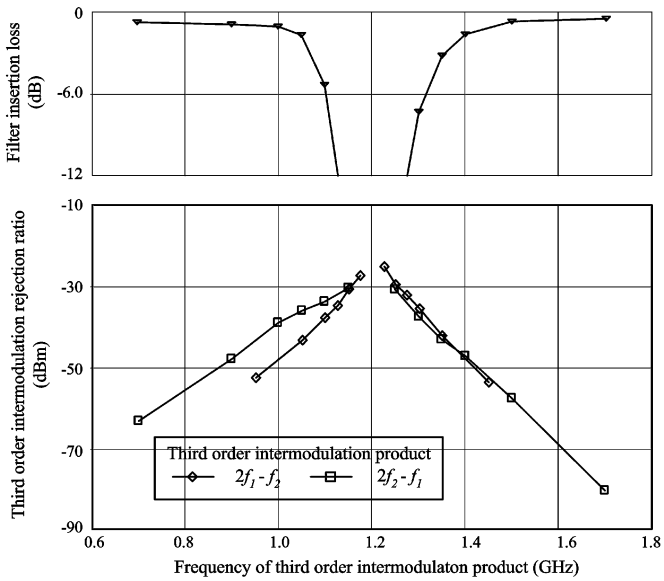

Fig. 12. Measured third-order IMD of a varactor-tuned BSF. The first tone, i.e., f_1, is held constant at the center of the stopband, while the second excitation tone, i.e., f_2, is swept above and below the first. The filter insertion loss is also shown.

the distortion is measured at the output of the filter; the distortion component at the output will be reduced in proportion to the filter stopband attenuation.

The third-order IMD performance of the BSF was also measured and the results are presented in Fig. 12. The measured results gave good agreement with the calculated results in Section III-C.2b. Below the filter stopband, the $2f_1 - f_2$ product decreases more rapidly than its counterpart, as predicted by the theoretical and measured results for the single resonator (Fig. 9). The quarter-wavelength frequency of the resonators in the measured filter were set to approximately 1.9 GHz; hence, the minima in the third-order distortion results are out of range in the case of the measured results.

V. Conclusion

The presented analysis has shown the distortion performance of two common varactor-tuned transmission-line configurations and the implications for tunable filter design.

Simple ac analysis on the parallel varactor transmission-line configuration, common in bandpass filters, reveals that the maximum signal voltage across the varactor diode occurs at the parallel resonant frequency. Thus, in a bandpass filter based on this configuration, maximum distortion will occur in the passband of the filter. This is demonstrated further through a Volterra-series analysis of the varactor-tuned parallel transmission-line resonator. Third-order distortion products are identified as being the most problematic for bandpass filters based on this topology and the third-order products are shown to be highest when the excitation signals are located in the passband.

Similar analysis of a series varactor-coupled transmission-line topology demonstrated that, when used as the building block in a BSF, much more favorable distortion characteristics are observed. In this case, maximum signal voltage across the varactor diode, and correspondingly, maximum distortion, will occur at the series resonant frequency. In a BSF based on this resonator configuration, this will correspond to the stopband of the filter. AC analysis also showed that the varactor voltage passes through a minimum at the transmission-line quarter-wavelength frequency. For the series configuration, this is significant since, in a BSF, the minimum-loss passband will occur at this frequency.

Volterra-series analysis of the varactor-tuned series transmission-line resonator showed that both the second- and third-order IMD products were at a maximum at the series resonant frequency. Notably, however, their magnitude passed through a minimum at the quarter-wavelength frequency (filter passband). The conclusion here is that, as long as the wanted signal is centred at the minimum-loss passband, varactor-tuned filters using this configuration may be useful in situations where only very low levels of distortion can be tolerated.

The nonlinear characteristics of bandpass and BSFs were measured in order to verify the analysis; good concurrence was shown between theoretical and measured results.

References

[1] D. Mirri, G. Iuculano, F. Filicori, G. Pasini, G. Vannini, and G. Gualtieri, "A modified Volterra series approach for nonlinear dynamic systems modelling," *IEEE Trans. Circuits Syst. I—Fundam. Theory Appl.*, vol. 49, no. 8, pp. 1118–1128, Aug. 2002.

[2] K. B. Ivlev, "Nonlinear distortions in passive varactor tunable resonators," in *Proc. IEEE–Russia High Power Microw. Electron.: Meas., Identification, Appl. Conf.*, 1999, pp. I34–I39.

[3] I. C. Hunter and S. R. Chandler, "Intermodulation distortion in active microwave filters," *Proc. Inst. Elect. Eng.—Microw., Antennas, Propag.*, vol. 145, no. 1, pp. 7–12, Feb. 1998.

[4] R. H. Caverly and G. Hiller, "Distortion in p-i-n diode control circuits," *IEEE Trans. Microw. Theory Tech.*, vol. MTT-35, no. 5, pp. 492–501, May 1987.

[5] *The PIN Diode Circuit Designer's Handbook*. Watertown, MA: Microsemi-Watertown, 1998.

[6] I. Bahl and P. Bhartia, *Microwave Solid State Circuit Design*. New York: Wiley, 1988.

[7] K. Buisman, L. de Vreede, L. Larson, M. Spirito, A. Akhnouk, T. Scholtes, and L. Nanver, "Distortion-free varactor diode topologies for RF adaptivity," IEEE MTT-S Int. Microw. Symp. Dig. Jun. 12–17, 2005, 4 pp.

[8] H. Dayal, "Variable bandwidth wide tunable frequency voltage tuned filter," *Int. J. RF Microw. Comput.-Aided Eng.*, vol. 14, no. 1, pp. 64–72, Jan. 2004.

[9] A. R. Brown and G. M. Rebeiz, "A varactor-tuned RF filter," *IEEE Trans. Microw. Theory Tech.*, vol. 48, no. 7, pp. 1157–1160, Jul. 2000.

[10] I. C. Hunter and J. D. Rhodes, "Electronically tunable microwave bandpass filters," *IEEE Trans. Microw. Theory Tech.*, vol. MTT-30, no. 9, pp. 1354–1360, Sep. 1982.

[11] S. Toyoda, "Quarter-wavelength coupled variable bandstop and bandpass filters using varactor modes," *IEEE Trans. Microw. Theory Tech.*, vol. MTT-30, no. 9, pp. 1387–1389, Sep. 1982.

[12] B. Carey-Smith and P. A. Warr, "Broadband configurable bandstop filter with composite tuning mechanism," *Electron. Lett.*, vol. 40, pp. 1587–1589, Dec. 2004.

[13] S. Maas, *Nonlinear Microwave Circuits*. Piscataway, NJ: IEEE Press, 1997, pp. 178–186.

[14] J. C. Pedro and N. Borges Carvalho, *Intermodulation Distortion in Microwave and Wireless Circuits*. Norwood, MA: Artech House, 2003.

Bruce E. Carey-Smith received the B.E. degree in electrical and electronic engineering from the University of Canterbury, Christchurch, New Zealand, in 1995, and is currently working toward the engineering Ph.D. degree at the University of Bristol, Bristol, U.K.

From 1995 to 2002, he was with Tait Electronics Ltd., Christchurch, New Zealand, where he was involved in the design of RF circuits and systems for mobile radio applications. He subsequently joined the University of Bristol, as a Research Associate with the Centre for Communications Research. His current research interests are in the areas of tunable microwave circuits and amplifier linearization for software reconfigurable radios.

Paul A. Warr received the B.Eng. degree in electronics and communications from The University of Bath, Bath, U.K., in 1994, and the M.Sc. degree in communications systems and signal processing and Ph.D. degree from The University of Bristol, U.K., in 1996 and 2001, respectively. His doctoral research concerned octave-band linear receiver amplifiers.

He is currently a Lecturer of radio frequency engineering with The University of Bristol. He was with the Marconi Company, where he was involved with secure high-redundancy cross-platform communications. His research concerns the front-end aspects of software (reconfigurable) radio and diversity-exploiting communication systems, responsive linear amplifiers, flexible filters, and linear frequency translation. His research has been funded by the U.K. Engineering and Physical Science Research Council (EPSRC) alongside the European Commission (EC) and industrial collaborators.

Dr. Warr is a member of the Executive Committee of the Institution of Electrical Engineers (IEE) Professional Network on Communication Networks and Services.